Computational Methods in Applied Mathematics
Vol. 14 (2014), No. 1, pp. 35–54

Doi: 10.1515/cmam-2013-0021

DE GRUYTER

Computational Survey on A Posteriori Error Estimators for the Crouzeix–Raviart Nonconforming Finite Element Method for the Stokes Problem

Carsten Carstensen · Christian Merdon

Abstract — This survey compares different strategies for guaranteed error control for the lowest-order nonconforming Crouzeix–Raviart finite element method for the Stokes equations. The upper error bound involves the minimal distance of the computed piecewise gradient $\mathrm{D}_{\mathrm{NC}}\, u_{\mathrm{CR}}$ to the gradients of Sobolev functions with exact boundary conditions. Several improved suggestions for the cheap computation of such test functions compete in five benchmark examples. This paper provides numerical evidence that guaranteed error control of the nonconforming FEM is indeed possible for the Stokes equations with overall efficiency indices between 1 to 4 in the asymptotic range.

2010 Mathematical subject classification: 65N30, 65N15.

Keywords: Nonconforming Finite Element Method, Crouzeix–Raviart Finite Element Method, Adaptive Finite Element Method, A Posteriori Error Estimation.

1. Introduction

The a posteriori error analysis of conforming FEM is well established and contained even in textbooks [3, 8, 9, 22]. Although a unified framework is established [11, 14], much less is known about a posteriori error analysis for nonconforming lowest-order Crouzeix–Raviart finite element methods [1,2,4,7,16,17]. This paper concerns the 2D Stokes equations: Given a right-hand side $f \in L^2(\Omega;\mathbb{R}^2)$ and Dirichlet data $u_D \in H^1(\Omega;\mathbb{R}^2)$ with $\int_{\partial\Omega} u_D \cdot \nu\, ds = 0$ (for the unit normal vector ν), seek a pressure $p \in L^2_0(\Omega) := \{q \in L^2(\Omega) \mid \int_\Omega q\, dx = 0\}$ and a velocity field $u \in H^1(\Omega;\mathbb{R}^2)$ with

$$-\Delta u + \nabla p = f \quad \text{and} \quad \operatorname{div} u = 0 \text{ in } \Omega \quad \text{while} \quad u = u_D \text{ on } \partial\Omega.$$

The primal variable u will be discretised with the nonconforming Crouzeix–Raviart FEM on some shape-regular triangulation $\mathcal{T}$ with discrete solution u_{CR}. This paper discusses and

Carsten Carstensen
Humboldt-Universität zu Berlin, Unter den Linden 6, 10099 Berlin, Germany; and
Department of Computational Science and Engineering, Yonsei University, 120-749 Seoul, Korea
E-mail: cc@mathematik.hu-berlin.de.

Christian Merdon
Weierstraß-Institut, Mohrenstr. 39, 10117 Berlin, Germany
E-mail: christian.merdon@wias-berlin.de.

compares different a posteriori error estimators for the error $e = u - u_{\mathrm{CR}}$ and its piecewise gradient $\mathrm{D}_{\mathrm{NC}}\, e$ in the (nonconforming) energy norm

$$|||e|||_{\mathrm{NC}}^2 := \|\mathrm{D}_{\mathrm{NC}}\, e\|_{L^2(\Omega)}^2 := \sum_{T\in\mathcal{T}} \|\mathrm{D}\, e\|_{L^2(T)}^2.$$

The decomposition from [2] allows for a split of this error into

$$|||e|||_{\mathrm{NC}}^2 \leqslant \eta^2 + \big(\|\mathrm{D}_{\mathrm{NC}}(u_{\mathrm{CR}} - v)\|_{L^2(\Omega)} + 1/c_0\, \|\mathrm{div}\, v\|_{L^2(\Omega)}\big)^2.$$

The first term on the right-hand side (with the first positive root $j_{1,1} \geqslant 3.8317$ of the first Bessel function J_1)

$$\eta := \|f_{\mathcal{T}}/2 \otimes (\bullet - \mathrm{mid}(\mathcal{T}))\|_{L^2(\Omega)} + 1/j_{1,1}\ \mathrm{osc}(f, \mathcal{T})$$

involves contributions of the data f and is directly computable (up to quadrature errors). The second term employs *any* $v \in H^1(\Omega;\mathbb{R}^2)$ with $v = u_D$ along $\partial\Omega$, e.g., componentwise interpolation by [1] or novel interpolations on the red-refined triangulation $\mathrm{red}(\mathcal{T})$ from [15]. The constant c_0 depends only on the domain Ω and equals the smallest eigenvalue of some general eigenvalue problem [19], cf. Section 3 below. This paper compares several possible designs of v and applies them in the five benchmark examples of Table 1.

Section	Short name	Problem data & features	c_0
5.1	Smooth Solution	$f \neq 0$, $u_D \neq 0$	0.3826
5.2	2nd Smooth Solution	$f \neq 0$, $u_D \neq 0$	0.3826
5.3	Colliding Flow	$f \equiv 0$, $u_D \neq 0$	0.3826
5.4	L-shaped Domain	$f \equiv 0$, $u_D \neq 0$, corner singularity	0.3
5.5	Backward Facing Step	$f \equiv 0$, $u_D \neq 0$, corner singularity	0.3

Table 1. Benchmark examples and section references.

The remaining parts of this paper are outlined as follows. Section 2 introduces the necessary notation, preliminaries and our adaptive mesh refinement algorithm. Section 3 presents the a posteriori error analysis and derivates a sharp upper bound for the energy error with explicit constants. Section 4 explains the realisation of the guaranteed upper bounds. Section 5 gives details on the error estimator competition for the five benchmark problems from Table 1. Section 6 draws some conclusions from the theoretical and numerical results of this paper.

Throughout this paper we use standard notation for Lebesgue and Sobolev spaces and their norms: $V := H_0^1(\Omega;\mathbb{R}^2)$ is endowed with the energy norm $|||\cdot||| := \|\nabla\cdot\|_{L^2(\Omega)} = |\cdot|_{H^1(\Omega)}$. Finally $a \lesssim b$ abbreviates $a \leqslant Cb$ for some generic constant C that depends only on the shape regularity of the triangulation while $a \approx b$ stands for $a \lesssim b \lesssim a$.

2. Notation and Preliminaries

2.1. Nonconforming Finite Element Spaces

Given a regular triangulation $\mathcal{T}$ of the bounded Lipschitz domain $\Omega \subseteq \mathbb{R}^2$ in the sense of Ciarlet into closed triangles with edges $\mathcal{E}$, nodes $\mathcal{N}$ and free nodes $\mathcal{M}$, the midpoints of all

edges are $\mathrm{mid}(\mathcal{E}) := \{\mathrm{mid}(E) \mid E \in \mathcal{E}\}$ and $\mathcal{E}(\partial\Omega)$ denotes the edges along the boundary $\partial\Omega$. The point $\mathrm{mid}(T)$ denotes the center of gravity of $T \in \mathcal{T}$ and defines the piecewise constant L^2 function $\mathrm{mid}(\mathcal{T}) \in P_0(\mathcal{T};\mathbb{R}^2)$ by $\mathrm{mid}(\mathcal{T})|_T = \mathrm{mid}(T)$ for all $T \in \mathcal{T}$. The set $\mathcal{E}(T)$ contains the three edges of a triangle $T \in \mathcal{T}$. With the elementwise first-order polynomials $P_1(\mathcal{T};\mathbb{R}^2)$, the nonconforming Crouzeix–Raviart finite element spaces are defined by

$$\mathrm{CR}^1(\mathcal{T};\mathbb{R}^2) := \big\{v \in P_1(\mathcal{T};\mathbb{R}^2) \mid v \text{ is continuous at } \mathrm{mid}(\mathcal{E})\big\},$$
$$\mathrm{CR}^1_0(\mathcal{T};\mathbb{R}^2) := \big\{v \in \mathrm{CR}^1(\mathcal{T};\mathbb{R}^2) \mid v(\mathrm{mid}(E)) = 0 \text{ for all } E \in \mathcal{E}(\partial\Omega)\big\}.$$

The Crouzeix–Raviart finite elements form a subspace of the broken Sobolev functions

$$H^1(\mathcal{T}) := \big\{v \in L^2(\Omega) \mid v|_T \in H^1(T) \text{ for all } T \in \mathcal{T}\big\}.$$

The diameter $\mathrm{diam}(T)$ of $T \in \mathcal{T}$ is denoted by h_T and $h_{\mathcal{T}}$ denotes their piecewise constant values with $h_{\mathcal{T}}|_T := h_T := \mathrm{diam}(T)$ for all $T \in \mathcal{T}$. The integral mean of a function $f \in L^2(\omega)$ (or any vector $f \in L^2(\omega;\mathbb{R}^2)$) over some open set ω is denoted by

$$f_\omega := \fint_\omega f\,dx := \int_\omega f\,dx/|\omega|.$$

The oscillations of $f \in L^2(\Omega)$ (as well as of vectors $f \in L^2(\Omega;\mathbb{R}^2)$) read

$$\mathrm{osc}(f,\mathcal{T}) := \Big(\sum_{T\in\mathcal{T}} \|h_T(f - f_T)\|^2_{L^2(T)}\Big)^{1/2} = \|h_{\mathcal{T}}(f - f_{\mathcal{T}})\|_{L^2(\Omega)}.$$

2.2. Crouzeix–Raviart FEM for the Stokes Equations

The discrete bilinear form reads

$$a_{\mathrm{NC}}(u_{\mathrm{CR}}, v_{\mathrm{CR}}) := \sum_{T\in\mathcal{T}} \int_T \mathrm{D}\,u_{\mathrm{CR}} : \mathrm{D}\,v_{\mathrm{CR}}\,dx$$

for all $u_{\mathrm{CR}}, v_{\mathrm{CR}} \in X_h := \mathrm{CR}^1(\mathcal{T};\mathbb{R}^2) \subseteq H^1(\mathcal{T};\mathbb{R}^2)$ with $A : B := \sum_{j,k=1,2} A_{jk}B_{jk}$ for all 2×2 matrices $A, B \in \mathbb{R}^{2\times 2}$. The particular choice of

$$Y_h := P_0(\mathcal{T}) \cap L^2_0(\Omega) \quad \text{and} \quad b_{\mathrm{NC}}(v,q) := \int_\Omega q\,\mathrm{div}_{\mathrm{NC}}\,v\,dx,$$

with the piecewise divergence operator $\mathrm{div}_{\mathrm{NC}}$, leads to the discrete counterpart

$$Z_{\mathrm{NC}} := \big\{v_{\mathrm{CR}} \in \mathrm{CR}^1_0(\mathcal{T};\mathbb{R}^2) \mid \mathrm{div}_{\mathrm{NC}}\,v_{\mathrm{CR}} = 0\big\}$$

of the space of divergence-free functions

$$Z := \big\{v \in H^1_0(\Omega;\mathbb{R}^2) \mid \mathrm{div}\,v = 0\big\}.$$

The nonconforming representation of the Stokes problem reads: Given $f \in L^2(\Omega;\mathbb{R}^2)$, seek $u_{\mathrm{CR}} \in \mathrm{CR}^1(\mathcal{T};\mathbb{R}^2)$ with $\mathrm{div}_{\mathrm{NC}}\,u_{\mathrm{CR}} = 0$,

$$u_{\mathrm{CR}}(\mathrm{mid}(E)) = \fint_E u_D\,ds \quad \text{for all } E \in \mathcal{E}(\partial\Omega),$$

and

$$a_{\rm NC}(u_{\rm CR}, v_{\rm CR}) = F(v_{\rm CR}) := \int_\Omega f \cdot v_{\rm CR}\, dx \quad \text{for all } v_{\rm CR} \in Z_{\rm NC}.$$

In other words, up to boundary conditions, $u_{\rm CR}$ is computed from the Riesz representation of a linear functional (given as right-hand side plus boundary modifications) in the Hilbert space $(Z_{\rm NC}, a_{\rm NC})$. The actual implementation uses unconstrained Crouzeix–Raviart elements $v_{\rm CR} \in {\rm CR}^1(\mathcal{T};\mathbb{R}^2)$ and another Lagrange multiplier to enforce the global constraint

$${\rm div}_{\rm NC}\, u_{\rm CR} = 0 \quad \text{a.e. in } \Omega.$$

2.3. Adaptive Mesh Refinement Algorithm

Algorithm 2.1 (ACRFEM)**.**
Input Coarse regular triangulation $\mathcal{T}_0$ and $0 < \Theta \leqslant 1$.
For level $\ell = 0, 1, 2, \ldots$ until termination do

Compute discrete solution $u_{\rm CR}$ on $\mathcal{T}_\ell$ with N_ℓ degrees of freedom. For any $v_{\rm xyz}$ for xyz $\in$ {A, PMA, MAred, PMred, MP1, MP2, MP2CG5, MP1red, MP1redCG3}, compute the refinement indicators

$$\begin{aligned}\eta_{\rm xyz}(T)^2 &:= \eta(T, v_{\rm xyz})^2 \\ &:= \big\|f_{\mathcal{T}}/2 \otimes (\bullet - {\rm mid}(T))\big\|^2_{L^2(T)} + 1/j_{1,1}^2 \big\|h_T(f - f_T)\big\|^2_{L^2(T)} \\ &\quad + \big\|{\rm D_{NC}}(u_{\rm CR} - v_{\rm xyz})\big\|^2_{L^2(T)} + 1/c_0^2 \big\|{\rm div}\, v_{\rm xyz}\big\|^2_{L^2(T)} \\ &\quad + (1 + 1/c_0^2) C_\gamma^2 \big\|h_{\mathcal{E}}^{3/2} \partial_{\mathcal{E}}^2 (u_D - v_{\rm xyz})/\partial s^2\big\|^2_{L^2(\partial\Omega\cap\partial T)}\end{aligned}$$

with C_γ from an estimate for inhomogeneous Dirichlet boundary data from Section 4.4. With the tangential jump $[{\rm D_{NC}}\, u_{\rm CR} \cdot \tau_E]_E$ for interior edges $E \in \mathcal{E} \setminus \mathcal{E}(\partial\Omega)$ and

$$[{\rm D_{NC}}\, u_{\rm CR} \cdot \tau_E]_E := \big\|\partial u_D/\partial s - {\rm D_{NC}}\, u_{\rm CR} \cdot \tau_E\big\|_{L^2(E)}$$

for boundary edges $E \in \mathcal{E}(\partial\Omega)$ with tangential vector τ_E, the residual-based refinement indicators read

$$\eta_{\rm R}(T)^2 := |T| \|f\|^2_{L^2(T)} + |T|^{1/2} \sum_{E\in\mathcal{E}(T)} \big\|[{\rm D_{NC}}\, u_{\rm CR} \cdot \tau_E]_E\big\|^2_{L^2(E)}.$$

Estimate

$$\begin{aligned}\eta(v_{\rm xyz})^2 := \Big(\big\|f_{\mathcal{T}}/2 \otimes (\bullet - {\rm mid}(\mathcal{T}))\big\|_{L^2(\Omega)} + 1/j_{1,1}\ {\rm osc}(f, \mathcal{T})\Big)^2 + \Big(\big\|{\rm D_{NC}}(u_{\rm CR} - v_{\rm xyz})\big\|_{L^2(\Omega)} \\ + 1/c_0 \,\|{\rm div}\, v_{\rm xyz}\|_{L^2(\Omega)} + (1 + 1/c_0) C_\gamma \big\|h_{\mathcal{E}}^{3/2} \partial_{\mathcal{E}}^2 (u_D - v_{\rm xyz})/\partial s^2\big\|_{L^2(\partial\Omega)}\Big)^2.\end{aligned}$$

Mark a minimal subset $\mathcal{M}_\ell$ of $\mathcal{T}_\ell$ (based on one set of refinement indicators) such that

$$\Theta \sum_{T\in\mathcal{T}_\ell} \eta_{\rm xyz}(T)^2 \leqslant \sum_{T\in\mathcal{M}_\ell} \eta_{\rm xyz}(T)^2.$$

Refine $\mathcal{T}_\ell$ by *red*-refinement of triangles in $\mathcal{M}_\ell$ and *red-green-blue*-refinement [10, 23] of further triangles to avoid hanging nodes and compute $\mathcal{T}_{\ell+1}$.

Output Sequence of meshes $\mathcal{T}_0, \mathcal{T}_1, \ldots$ with respective discrete solution u_{CR} and residual-based error estimator

$$\eta_{\mathrm{R}}(\mathcal{T}_\ell) := \|h_{\mathcal{T}_\ell} f\|_{L^2(\Omega)} + \Big(\sum_{E \in \mathcal{E}_\ell} |E| \, \big\| [\mathrm{D}_{\mathrm{NC}} u_{\mathrm{CR}} \cdot \tau_E]_E \big\|^2_{L^2(E)} \Big)^{1/2}.$$

3. A Posteriori Error Estimation for Stokes Equations

This section is devoted to guaranteed upper bounds for the error in the nonconforming energy norm for the Stokes problem based on a decomposition from [2] with a slightly sharper upper bound. The general reliability result involves the computable term

$$\eta := \big\| f_{\mathcal{T}}/2 \otimes (\bullet - \mathrm{mid}(\mathcal{T})) \big\|_{L^2(\Omega)} + 1/j_{1,1} \, \mathrm{osc}(f, \mathcal{T}).$$

Here, $j_{1,1}$ is the first positive root of the first Bessel function J_1 and, for two vectors $x, y \in \mathbb{R}^2$, $x \otimes y := (x_1 y_1, x_1 y_2; x_2 y_1, x_2 y_2) \in \mathbb{R}^{2\times 2}$ denotes their dyadic product. For every triangle $T \in \mathcal{T}$ with the set of its edges $\mathcal{E}(T)$ and $s(T)^2 := \sum_{E \in \mathcal{E}(T)} |E|^2$, an elementary calculation shows

$$\big\| f_{\mathcal{T}}/2 \otimes (\bullet - \mathrm{mid}(\mathcal{T})) \big\|^2_{L^2(T)} := |f_{\mathcal{T}}/2|^2 \big\| \bullet - \mathrm{mid}(\mathcal{T}) \big\|^2_{L^2(T)} = |f_{\mathcal{T}}|^2 |T| s(T)^2/144.$$

The constant c_0 in the inf-sup condition

$$0 < c_0 := \inf_{q \in L^2_0(\Omega)} \sup_{v \in H^1(\Omega;\mathbb{R}^2)/\mathbb{R}^2} \frac{\int_\Omega q \, \mathrm{div}(v) \, dx}{\|\mathrm{D}\, v\|_{L^2(\Omega)} \|q\|_{L^2(\Omega)}}$$

depends only on the domain Ω and equals the smallest eigenvalue of some general eigenvalue problem [19]. Their values are given in Table 1.

The following a posteriori error estimate resembles the upper bound from [2, Theorem 1]

$$\begin{aligned} |||e|||_{\mathrm{NC}} \leqslant \big\| f_{\mathcal{T}}/2 \otimes (\bullet - \mathrm{mid}(\mathcal{T})) \big\|_{L^2(\Omega)} + C \, \mathrm{osc}(f, \mathcal{T}) \\ + \big\| \mathrm{D}_{\mathrm{NC}}(u_{\mathrm{CR}} - v) \big\|_{L^2(\Omega)} + 1/c_0 \, \|\mathrm{div}\, v\|_{L^2(\Omega)} \end{aligned} \tag{3.1}$$

and gives a refined version with an explicit value for C.

Theorem 3.1. *Any $v \in H^1(\Omega;\mathbb{R}^2)$ with $v = u_D$ on $\partial\Omega$ satisfies*

$$|||e|||^2_{\mathrm{NC}} \leqslant \eta^2 + \big(\big\| \mathrm{D}_{\mathrm{NC}}(u_{\mathrm{CR}} - v) \big\|_{L^2(\Omega)} + 1/c_0 \, \|\mathrm{div}\, v\|_{L^2(\Omega)} \big)^2. \tag{3.2}$$

Proof. The analysis follows [2] and is repeated here for convenient reading to stress the little differences to [2, Theorem 1]. These differences concern the powers in (3.2) compared to (3.1), which lead to a sharper guaranteed upper bound, and the explicitly given constant in (3.5). The point of departure is the orthogonal split

$$\mathrm{D}_{\mathrm{NC}}\, e = \mathrm{D}\, z + y$$

into $z \in Z$ with

$$\int_\Omega \mathrm{D}\, z : \mathrm{D}\, v \, dx = \int_\Omega \mathrm{D}_{\mathrm{NC}}\, e : \mathrm{D}\, v \, dx \quad \text{for all } v \in Z,$$

and the remainder

$$y \in Y := \Big\{ y \in L^2(\Omega;\mathbb{R}^{2\times 2}) \mid \int_\Omega y : \mathrm{D}\, v \, dx = 0 \text{ for all } v \in Z \Big\}.$$

Orthogonality holds in the sense of

$$|||e|||_{\mathrm{NC}}^2 = |||z|||_{\mathrm{NC}}^2 + \|y\|_{L^2(\Omega)}^2 = \int_\Omega \mathrm{D}_{\mathrm{NC}}\, e : \mathrm{D}\, z \, dx + \int_\Omega \mathrm{D}_{\mathrm{NC}}\, e : y \, dx.$$

To estimate $\int_\Omega \mathrm{D}_{\mathrm{NC}}\, e : \mathrm{D}\, z \, dx$, employ the nonconforming interpolation $z_{\mathrm{NC}} \in \mathrm{CR}^1(\mathcal{T};\mathbb{R}^2)$ of z defined by

$$z_{\mathrm{NC}}(\mathrm{mid}(E)) := \fint_E z \, ds \quad \text{for all } E \in \mathcal{E}.$$

An integration by parts yields $z_{\mathrm{NC}} \in Z_{\mathrm{NC}}$ and

$$\int_T \mathrm{D}(z - z_{\mathrm{NC}}) \, dx = 0 \quad \text{for all } T \in \mathcal{T}. \tag{3.3}$$

This allows for the following computation:

$$\begin{aligned} \int_\Omega \mathrm{D}_{\mathrm{NC}}\, e : \mathrm{D}\, z \, dx &= F(z) - a_{\mathrm{NC}}(u_{\mathrm{CR}}, z) \\ &= F(z - z_{\mathrm{NC}}) - a_{\mathrm{NC}}(u_{\mathrm{CR}}, z) + F(z_{\mathrm{NC}}) \\ &= \int_\Omega f \cdot (z - z_{\mathrm{NC}}) \, dx - a_{\mathrm{NC}}(u_{\mathrm{CR}}, z - z_{\mathrm{NC}}). \end{aligned}$$

Equation (3.3) and $\nabla u_{\mathrm{CR}} \in P_0(\mathcal{T};\mathbb{R}^{2\times 2})$ yield $a_{\mathrm{NC}}(u_{\mathrm{CR}}, z - z_{\mathrm{NC}}) = 0$. Hence,

$$\begin{aligned} \int_\Omega \mathrm{D}_{\mathrm{NC}}\, e : \mathrm{D}\, z \, dx &= \int_\Omega f \cdot (z - z_{\mathrm{NC}}) \, dx \\ &= \int_\Omega f_{\mathcal{T}} \cdot (z - z_{\mathrm{NC}}) \, dx + \int_\Omega (f - f_{\mathcal{T}}) \cdot (z - z_{\mathrm{NC}}) \, dx. \end{aligned} \tag{3.4}$$

For every $T \in \mathcal{T}$, consider the function $q_{\mathcal{T}}|_T \in H(\mathrm{div}, T;\mathbb{R}^{2\times 2})$ defined by

$$q_{\mathcal{T}}(x)|_T := -f_{\mathcal{T}}/2 \otimes (x - \mathrm{mid}(T)) \quad \text{for } x \in T.$$

An integration by parts and some basic calculations show, for any $v \in H_0^1(\Omega;\mathbb{R}^2)$, that

$$\begin{aligned} \int_T q_{\mathcal{T}} : \nabla v \, dx &= \int_{\partial T} q_{\mathcal{T}} \nu \cdot v \, ds - \int_T \mathrm{div}\, q_{\mathcal{T}} \cdot v \, dx \\ &= -\sum_{E \in \mathcal{E}(\partial T)} f_{\mathcal{T}} |T| / (3|E|) \int_E v \, ds + \int_T f_{\mathcal{T}} \cdot v \, dx \\ &= \int_T f_{\mathcal{T}} \cdot (v - v_{\mathrm{NC}}) \, dx. \end{aligned}$$

Moreover, the $P_0(\mathcal{T})$ orthogonality of $f - f_\mathcal{T}$ and a Poincaré inequality with constant $\operatorname{diam}(T)/j_{1,1}$ from [18] yield

$$\begin{aligned}\int_\Omega (f - f_\mathcal{T}) \cdot (z - z_{\mathrm{NC}})\, dx &= \int_\Omega (f - f_\mathcal{T}) \cdot (z - z_{\mathrm{NC}} - (z - z_{\mathrm{NC}})_\mathcal{T})\, dx \\ &\leqslant \sum_{T\in\mathcal{T}} \|f - f_\mathcal{T}\|_{L^2(T)} \|z - z_{\mathrm{NC}} - (z - z_{\mathrm{NC}})_\mathcal{T}\|_{L^2(T)} \\ &\leqslant 1/j_{1,1}\ \operatorname{osc}(f,\mathcal{T}) \|\mathrm{D}(z - z_{\mathrm{NC}})\|_{L^2(\Omega)}. \end{aligned} \tag{3.5}$$

Hence, (3.4) reads

$$\begin{aligned}\int_\Omega \mathrm{D}_{\mathrm{NC}}\, e : \mathrm{D}\, z\, dx &= \int_\Omega q_\mathcal{T} : \nabla z\, dx + \int_\Omega (f - f_\mathcal{T}) \cdot (z - z_{\mathrm{NC}})\, dx \\ &\leqslant \|q_\mathcal{T}\|_{L^2(\Omega)} |||z|||_{\mathrm{NC}} + 1/j_{1,1}\ \operatorname{osc}(f,\mathcal{T}) |||z - z_{\mathrm{NC}}|||_{\mathrm{NC}}.\end{aligned}$$

Notice that (3.3) yields

$$\begin{aligned}\|\mathrm{D}(z - z_{\mathrm{NC}})\|^2_{L^2(T)} &= \int_T |\mathrm{D}\, z|^2\, dx - 2\int_T \mathrm{D}\, z : \mathrm{D}\, z_{\mathrm{NC}}\, dx + \int_T |\mathrm{D}\, z_{\mathrm{NC}}|^2\, dx \\ &= \int_T |\mathrm{D}\, z|^2\, dx - \int_\Omega |\mathrm{D}\, z_{\mathrm{NC}}|^2\, dx \leqslant \|\mathrm{D}\, z\|^2_{L^2(T)}.\end{aligned}$$

It remains to estimate $\int_\Omega \mathrm{D}_{\mathrm{NC}}\, e : y\, dx$. Recall from [2] that, for each $y \in Y$, there exists some

$$w \in L^2_0(\Omega) := \Big\{ q \in L^2(\Omega) \mid \int_\Omega q\, dx = 0 \Big\}$$

with

$$\int_\Omega y : \mathrm{D}\, v\, dx = \int_\Omega w \operatorname{div} v\, dx \quad \text{for all } v \in H^1(\Omega;\mathbb{R}^2)$$

and

$$\|w\|_{L^2(\Omega)} \leqslant 1/c_0\, \|y\|_{L^2(\Omega)}.$$

Hence, given any $v \in H^1(\Omega;\mathbb{R}^2)$ with $u - v = 0$ on $\partial\Omega$, it holds

$$\begin{aligned}\int_\Omega \mathrm{D}_{\mathrm{NC}}\, e : y\, dx &= \int_\Omega \mathrm{D}_{\mathrm{NC}}(u_{\mathrm{CR}} - v) : y\, dx + \int_\Omega \mathrm{D}(v - u) : y\, dx \\ &\leqslant \big\|\mathrm{D}_{\mathrm{NC}}(u_{\mathrm{CR}} - v)\big\|_{L^2(\Omega)} \|y\|_{L^2(\Omega)} + \int_\Omega \operatorname{div}(v - u) w\, dx \\ &\leqslant \big(\big\|\mathrm{D}_{\mathrm{NC}}(u_{\mathrm{CR}} - v)\big\|_{L^2(\Omega)} + 1/c_0\, \|\operatorname{div} v\|_{L^2(\Omega)}\big) \|y\|_{L^2(\Omega)}.\end{aligned}$$

The combination of all mentioned results concludes the proof. □

4. Realisations of Guaranteed Upper Bounds

The subsequent Sections 4.1–4.3 discuss nine designs for v and the estimation of $|||e|||$ via Theorem 3.1 with

$$\mu(v) := \|\mathrm{D}_{\mathrm{NC}}(u_{\mathrm{CR}} - v)\|_{L^2(\Omega)} + 1/c_0\, \|\operatorname{div} v\|_{L^2(\Omega)}. \tag{4.1}$$

The significant difference to [15] on the Poisson problem lies in the additional divergence term which leads to a sum of L^2 norms and Algorithms 4.1 and 4.2.

4.1. Interpolation after Ainsworth

This subsection introduces the interpolation after Ainsworth [1] that designs some piecewise linear $v_{\mathrm{A}} \in H^1(\Omega;\mathbb{R}^2)$ with respect to the original triangulation $\mathcal{T}$,

$$v_{\mathrm{A}}(z) := \begin{cases} u_D(z) & \text{if } z \in \mathcal{N} \setminus \mathcal{M}, \\ \big(\sum_{T\in\mathcal{T}(z)} u_{\mathrm{CR}}|_T(z)\big)/|\mathcal{T}(z)| & \text{if } z \in \mathcal{M}. \end{cases}$$

Here, the set $\mathcal{T}(z) := \{T \in \mathcal{T} \mid z \in T\}$ contains the triangles adjacent to $z \in \mathcal{N}$. The related error estimator reads

$$\eta_{\mathrm{A}}^2 := \eta^2 + \mu(v_{\mathrm{A}})^2.$$

4.2. Modified Interpolation Operator

This subsection introduces an improved interpolation that designs some piecewise linear $v_{\mathrm{red}} \in H^1_0(\Omega;\mathbb{R}^2)$ with respect to the red refined triangulation $\mathrm{red}(\mathcal{T})$. The red refinement connects the three edge midpoints $\mathrm{mid}(\mathcal{E}(T))$ within every triangle $T \in \mathcal{T}$ and so divides every triangle into four triangles with the same area. The nodes of $\mathrm{red}(\mathcal{T})$ consist of the original nodes $\mathcal{N}$ and the edge midpoints $\mathrm{mid}(\mathcal{E})$ of $\mathcal{T}$. At the boundary the interpolation equals the nodal interpolation of u_D and on all interior edge midpoints it equals u_{CR};

$$v_{\mathrm{red}}(z) := \begin{cases} u_{\mathrm{CR}}(z) & \text{for } z \in \mathrm{mid}(\mathcal{E}) \setminus \mathrm{mid}(\mathcal{E}(\partial\Omega)), \\ u_D(z) & \text{for } z \in (\mathcal{N} \cup \mathrm{mid}(\mathcal{E})) \cap \partial\Omega, \\ v_z & \text{for } z \in \mathcal{M}. \end{cases} \tag{4.2}$$

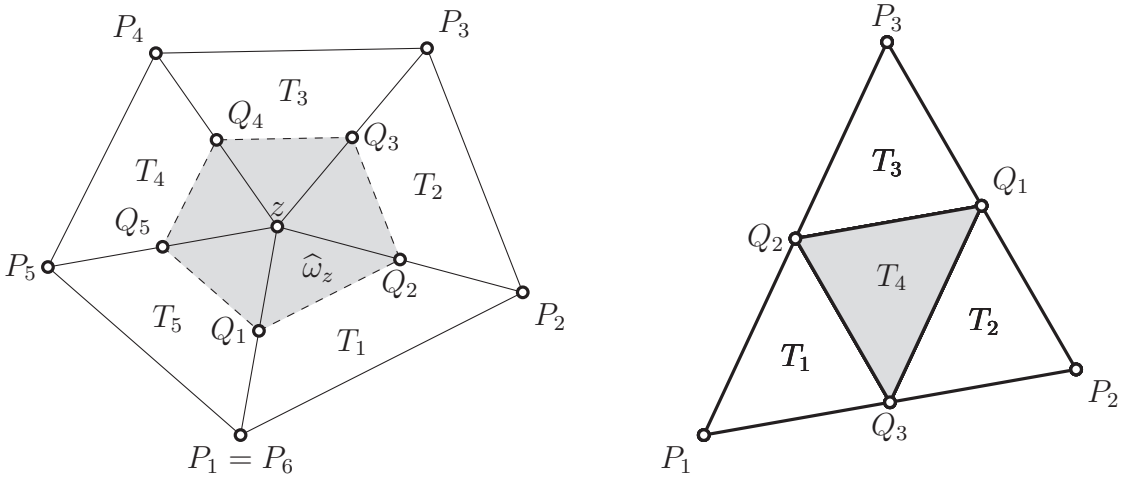

(a) Interior patch

(b) Central subtriangle $T_4 = \mathrm{conv}\{\mathrm{mid}(\mathcal{E}(T))\}$ in $\mathrm{red}(T)$ for $T \in \mathcal{T}$.

Figure 1. Notation for red-refinements.

In this way, the interpolation v_{red} equals u_{CR} on all central subtriangles like T_4 in Figure 1 (b) and it remains to determine the values v_z at the free nodes $z \in \mathcal{M}$. They may be chosen as in the design of v_{A}, but we suggest to choose them locally optimal with Algorithm 4.1 by solving local problems around each node patch $\widehat{\omega}_z$ with respect to the red-refined triangulation as in Figure 1 (a) under the side condition of the fixed values at the

edge midpoints Q_j of the adjacent edges with the corresponding nodal basis functions $\varphi^{\mathrm{red}}_{Q_j}$ with respect to the red-refined triangulation. The value v_z at z remains the only degree of freedom in this local problem.

Algorithm 4.1 (Patchwise minimisation)**.**

Input $u_{\mathrm{CR}} \in \mathrm{CR}^1(\mathcal{T};\mathbb{R}^2)$ and $c_0 > 0$. Set $\lambda := 1$.

For $j = 1, 2, \ldots$ until termination compute (a) and (b):

(a) For all $z \in \mathcal{N}(\Omega)$,

$$\begin{aligned} v_0 &:= \sum_{E\in\mathcal{E}} v_{\mathrm{red}}(\mathrm{mid}(E))\varphi^{\mathrm{red}}_{\mathrm{mid}(E)},\\ v_z &:= \operatorname*{argmin}_{w\in\mathbb{R}^2}\Big((1+\lambda)\big\|\mathrm{D_{NC}}(u_{\mathrm{CR}} - v_0 - w\varphi^{\mathrm{red}}_z)\big\|^2_{L^2(\widehat{\omega}_z)}\\ &\qquad\qquad + (1+1/\lambda)/c_0^2\,\big\|\mathrm{div}(v_0 - w\varphi^{\mathrm{red}}_z)\big\|^2_{L^2(\widehat{\omega}_z)}\Big). \end{aligned}$$

(b) Update

$$\begin{aligned} v_{\mathrm{red}} &:= v_0 + \sum_{z\in\mathcal{N}(\Omega)} v_z\varphi^{\mathrm{red}}_z,\\ \lambda &:= \|\mathrm{div}\, v_{\mathrm{red}}\|_{L^2(\Omega)}/\big(c_0\big\|\mathrm{D_{NC}}(u_{\mathrm{CR}} - v_{\mathrm{red}})\big\|_{L^2(\Omega)}\big),\\ \eta^2_{\mathrm{PMred}(j)} &:= \eta^2 + \mu(v_{\mathrm{red}})^2. \end{aligned}$$

Output $\eta_{\mathrm{PMred}(j)}$ for $j = 1, 2, \ldots$

We distinguish between the optimal version $\eta_{\mathrm{PMred}(j)}$ from Algorithm 4.1, and η_{MAred} with the suboptimal choice v_z as in Section 4.1. This can be seen as a modification v_{MAred} of v_{A} at the edge midpoints.

Some numerical examples below suggest that the fixed values at the edge midpoints from v_{red} lead to unexpectedly large divergence terms. Indeed, even the interpolation v_{A} may lead to better results than v_{MAred} on fine meshes as displayed in Section 5.4. Of course, it is possible to describe other values at the edge midpoints and substitute (4.2) by, e.g.,

$$v_{\mathrm{red}}(z) := \begin{cases} v_{\mathrm{A}}(z) & \text{for } z \in \mathrm{mid}(\mathcal{E}) \setminus \mathrm{mid}(\mathcal{E}(\partial\Omega)),\\ u_D(z) & \text{for } z \in (\mathcal{N} \cup \mathrm{mid}(\mathcal{E})) \cap \partial\Omega,\\ v_z & \text{for } z \in \mathcal{M}. \end{cases} \tag{4.3}$$

The optimal value v_z can again be computed similar to Algorithm 4.1 with v_{red} replaced by v_{A} and output $\eta_{\mathrm{PMA}(j)}$. Since $v_z = v_{\mathrm{A}}(z)$ is admissible in this optimisation, $\eta_{\mathrm{PMA}(j)}$ can only lead to better results than the interpolation η_{A}.

Table 2 compares the outcome $\eta_{\mathrm{PMred}(j)}$ (resp. $\eta_{\mathrm{PMA}(j)}$) of Algorithm 4.1 for $j = 1, 2, 3, 5, 10$ with the edge values (4.2) (resp. (4.3)). There is no significant improvement for coarse meshes and only little improvement on fine meshes. Surprisingly, the design of η_{PMA} is somehow insensitive for $j \geqslant 2$ in Algorithm 4.1.

ndof	13	57	241	993	4033	16257	65281	261633
η_{A}	1817.92	699.646	276.868	112.429	46.5926	19.7549	8.59524	3.83932
$\eta_{\mathrm{PMA}(1)}$	719.926	290.836	131.632	61.9372	29.1130	13.6895	6.48276	3.10096
$\eta_{\mathrm{PMA}(2)}$	719.926	290.773	131.611	61.9337	29.1126	13.6894	6.48274	3.10096
$\eta_{\mathrm{PMA}(3)}$	719.926	290.773	131.611	61.9337	29.1126	13.6894	6.48274	3.10096
$\eta_{\mathrm{PMA}(4)}$	719.926	290.773	131.611	61.9337	29.1126	13.6894	6.48274	3.10096
$\eta_{\mathrm{PMA}(5)}$	719.926	290.773	131.611	61.9337	29.1126	13.6894	6.48274	3.10096
η_{MAred}	719.926	286.729	122.127	55.5387	25.5059	11.7695	5.48898	2.59459
$\eta_{\mathrm{PMred}(1)}$	719.926	286.684	121.653	54.4621	24.4546	11.0798	5.10119	2.39005
$\eta_{\mathrm{PMred}(2)}$	719.926	286.677	121.632	54.4186	24.4286	11.0678	5.09563	2.38739
$\eta_{\mathrm{PMred}(3)}$	719.926	286.677	121.632	54.4183	24.4281	11.0674	5.09542	2.38728
$\eta_{\mathrm{PMred}(4)}$	719.926	286.677	121.632	54.4183	24.4281	11.0674	5.09542	2.38728
$\eta_{\mathrm{PMred}(5)}$	719.926	286.677	121.632	54.4183	24.4281	11.0674	5.09542	2.38728

Table 2. Error estimators η_{A}, η_{MAred}, $\eta_{\mathrm{PMA}(j)}$ and $\eta_{\mathrm{PMred}(j)}$ for $j = 1, 2, 3, 5, 10$ in Algorithm 4.1 and uniform mesh refinement in the example of Section 5.3 (with Dirichlet data error contribution from Section 4.4).

4.3. Optimal Choices

The global minimisers v_{MP1} in $P_1(\mathcal{T})\cap C(\Omega)$, v_{MP2} in $P_2(\mathcal{T})\cap C(\Omega)$ and v_{MP1red} in $P_1(\mathrm{red}(\mathcal{T}))\cap C(\Omega)$ on the red-refined triangulation $\mathrm{red}(\mathcal{T})$ of the functional μ from (4.1) are computed by Algorithm 4.2.

Algorithm 4.2 (Global minimisation)**.**

Input $u_{\mathrm{CR}} \in \mathrm{CR}^1(\mathcal{T};\mathbb{R}^2)$, $W(\mathcal{T}) \in \{P_1(\mathcal{T}) \cap C(\Omega), P_1(\mathrm{red}(\mathcal{T})) \cap C(\Omega), P_2(\mathcal{T}) \cap C(\Omega)\}$ and $c_0 > 0$. Set $\lambda := 1$.

For $j = 1, 2, \ldots$ until termination do

$$v_{W(\mathcal{T})} := \operatorname*{argmin}_{v\in W(\mathcal{T})}\big((1+\lambda)\big\|\mathrm{D}_{\mathrm{NC}}(u_{\mathrm{CR}}-v)\big\|^2_{L^2(\Omega)} + (1+1/\lambda)\|\operatorname{div} v\|^2_{L^2(\Omega)}/c_0^2\big), \tag{4.4}$$

$$\eta^2_{j,W(\mathcal{T})} := \eta^2 + \mu(v_{W(\mathcal{T})})^2,$$

$$\lambda := \|\operatorname{div} v_{W(\mathcal{T})}\|_{L^2(\Omega)}/\big(c_0\big\|\mathrm{D}_{\mathrm{NC}}(u_{\mathrm{CR}} - v_{W(\mathcal{T})})\big\|_{L^2(\Omega)}\big).$$

Output $\eta_{\mathrm{MP1}(j)} := \eta_{j,P_1(\mathcal{T})\cap C(\Omega)}$, $\eta_{\mathrm{MP1red}(j)} := \eta_{j,P_1(\mathrm{red}(\mathcal{T}))\cap C(\Omega)}$, $\eta_{\mathrm{MP2}(j)} := \eta_{j,P_2(\mathcal{T})\cap C(\Omega)}$ for $j = 1, 2, \ldots$

Table 3 displays values of $\eta_{\mathrm{MP2}(j)}$ for $j = 1, 2, \ldots, 5$ and suggests that there is a more significant improvement by Algorithm 4.2 compared to Algorithm 4.1 for the local designs. In the computational examples of Section 5, the termination of Algorithms 4.1 and 4.2 is with $j = 3$.

To reduce the computational costs of (4.4) one might use v_{MAred} as an initial guess for some iterative solver to draw near the minimiser of (4.4) for $W(\mathcal{T}) = P_1(\mathrm{red}(\mathcal{T})) \cap C(\Omega)$. We use a preconditioned conjugate gradients scheme and stop at the third iterate. The preconditioner is the diagonal of the system matrix named after Jacobi. This approximation of (4.4) in Algorithm 4.2 with $j = 3$ results in the estimator $\eta_{\mathrm{MP1redCG3}}$. Similarly, the nodal values of v_{MAred} define some piecewise quadratic function and hence an initial value for some PCG algorithm for the approximation of the minimiser of (4.4) for $W(\mathcal{T}) = P_2(\mathcal{T})\cap C(\Omega)$. The truncation of the minimisation in (4.4) after five PCG iterations and $j = 3$ in Algorithm 4.2 defines the error estimator η_{MP2CG5}.

ndof	13	57	241	993	4033	16257	65281	261633
$\eta_{\mathrm{MP2}(1)}$	516.780	171.508	50.5265	18.2578	7.88212	3.72095	1.82154	0.903860
$\eta_{\mathrm{MP2}(2)}$	516.747	169.398	49.1931	17.2531	7.24667	3.36511	1.63548	0.809433
$\eta_{\mathrm{MP2}(3)}$	516.747	169.159	48.9606	17.1022	7.14785	3.30029	1.59558	0.787235
$\eta_{\mathrm{MP2}(4)}$	516.747	169.144	48.9070	17.0820	7.13818	3.29419	1.59092	0.783648
$\eta_{\mathrm{MP2}(5)}$	516.747	169.143	48.8919	17.0791	7.13742	3.29387	1.59069	0.783424

Table 3. Error estimator $\eta_{\mathrm{MP2}(j)}$ for $j = 1, \ldots, 5$ in Algorithm 4.2 and uniform mesh refinement in the example of Section 5.3 (with Dirichlet data error contribution from Section 4.4).

Remark 4.1. The Algorithms 4.1 and 4.2 approximate the minimum of $\mu(v)$ amongst $v \in W(\mathcal{T})$ by a series of quadratic minimisation problems based on the identity

$$\min_{v\in W(\mathcal{T})} \mu(v) = \min_{\lambda\in\mathbb{R}} \min_{v\in W(\mathcal{T})} \big((1+\lambda)\big\|\mathrm{D}_{\mathrm{NC}}(u_{\mathrm{CR}}-v)\big\|^2_{L^2(\Omega)} + (1+1/\lambda)\|\operatorname{div} v\|^2_{L^2(\Omega)}/c_0^2\big)$$

and alternating direction minimisation in the variable v and λ.

4.4. Inhomogeneous Dirichlet Boundary Conditions

In case of inhomogeneous boundary conditions, the designs of v_{xyz} from the previous subsections do not satisfy $u - v_{\mathrm{xyz}} = 0$ on $\partial\Omega$ in general. To overcome this difficulty consider $w_D \in H^1(\Omega;\mathbb{R}^2)$ from [6, 15] with

$$w_D|_{\partial\Omega} = u_D|_{\partial\Omega} - v_{\mathrm{xyz}}|_{\partial\Omega}.$$

Then, Theorem 3.1 for $v = v_{\mathrm{xyz}} - w_D$ yields $u - v \in H^1_0(\Omega)$ and

$$\begin{aligned}|||e|||^2_{\mathrm{NC}} &\leqslant \eta^2 + \big(\big\|\mathrm{D}_{\mathrm{NC}}(u_{\mathrm{CR}}-v-w_D)\big\|_{L^2(\Omega)} + 1/c_0\,\big\|\operatorname{div}(v+w_D)\big\|_{L^2(\Omega)}\big)^2\\ &\leqslant \eta^2 + \big(\big\|\mathrm{D}_{\mathrm{NC}}(u_{\mathrm{CR}}-v)\big\|_{L^2(\Omega)} + 1/c_0\,\|\operatorname{div} v\|_{L^2(\Omega)} + (1+1/c_0)|||w_D|||\big)^2.\end{aligned}$$

In case of $v_{\mathrm{xyz}}|_{\partial\Omega} = \mathcal{I}u_D|_{\partial\Omega} := \sum_{z\in\mathcal{N}\setminus\mathcal{M}} u_D(z)\varphi_z|_{\partial\Omega}$, it holds [6, 15]

$$|||w_D||| \leqslant C_\gamma \big\|h_{\mathcal{E}}^{3/2}\partial^2_{\mathcal{E}}(u_D - v_{\mathrm{xyz}})/\partial s^2\big\|_{L^2(\partial\Omega)}.$$

Remark 4.2 ([15])**.** For right isosceles triangles numerical calculations suggest the constant $C_\gamma = 0.4980$. If $v_{\mathrm{xyz}}|_{\partial\Omega}$ is the nodal interpolation of $u_D|_{\partial\Omega}$ on the red-refined triangulation, w_D can be designed on the red-refined triangulation with halved edge lengths and the constant reduces to $C_\gamma = 0.4980/2^{3/2} = 0.1761$. The same holds if v_{xyz} equals the P_2 interpolation of u_D on $\mathcal{T}$ along $\partial\Omega$.

5. Numerical Experiments

This section discusses the five benchmark examples from Table 1.

5.1. Smooth Example

The first benchmark problem employs the right-hand side $f(x,y) = (4\pi^2 \sin(\pi(x-y)), 0)$ and inhomogeneous Dirichlet boundary data u_D with exact solution

$$u(x,y)_j = \sin(\pi x)\cos(\pi y) - \cos(\pi x)\sin(\pi y) \quad \text{for } j = 1,2$$

on the square domain $\Omega = (-1,1)^2$ with $c_0 = 0.3826$ from [19].

Figure 2 shows the efficiency indices in case of uniform and adaptive mesh refinement in the range of 1 to 3. While η_{MAred} is superior to η_{A} in case of Poisson problems from [15], this example shows that this must not be the case for Stokes problems. The piecewise minimal improvement η_{PMred} closes the gap between η_{A} and η_{MAred}, but barely leads to more efficient upper bounds than η_{A} at least for uniform mesh refinement. Here, η_{PMA} performs better and converges to efficiency indices close to 1.5 for uniform mesh refinement and efficiency indices below 2.5 for adaptive mesh refinement. The error estimator $\eta_{\mathrm{MP1redCG3}}$ and its optimal limit η_{MP1red} with efficiency indices between 1.25 and 1.75 only lose to η_{MP2} which allows for efficiency indices close to 1. The residual error estimator η_{R} with efficiency indices above 8 is not displayed. Figure 3 shows that none of the error estimators leads to significantly better refined meshes.

5.2. Second Smooth Example

The second benchmark problem from [2] employs the right-hand side $f(x,y) = (-4y, 4x)$ and inhomogeneous Dirichlet boundary data u_D that matches the exact solution

$$u(x,y) = [x(1-x)(1-2y), -y(1-y)(1-2x)]$$

on the square domain $\Omega = (0,1)^2$ with $c_0 = 0.3826$ from [19]. Since u is smooth, the convergence rates for the energy error are optimal for uniform and adaptive mesh refinement as depicted in Figure 5.

The efficiency indices displayed in Figure 4 scatter more than in the first example. The error estimators η_{MP1} and η_{A} yield almost identical efficiency indices larger than 5 for uniform mesh refinement. The red($\mathcal{T}$)-based interpolation error estimators η_{MAred} and η_{PMred} yield efficiency indices of about 3, while η_{MP1red} and $\eta_{\mathrm{MP1redCG3}}$ allow efficiency indices around 2. Again, the most accurate error estimators are η_{MP2} and η_{MP2CG5}.

5.3. Colliding Flow Example

The third benchmark problem employs $f(x,y) \equiv 0$ and the exact solution $u(x,y) = (20xy^4 - 4x^5, 20x^4y - 4y^5)$ on the square domain $\Omega = (-1,1)^2$ with $c_0 = 0.3826$ from [19]. This is another smooth example with optimal convergence rates of the energy error for uniform and adaptive mesh refinement as shown in Figure 7.

The efficiency indices for adaptive mesh refinement displayed in Figure 6 are in the range between almost 1 in case of η_{MP2} and 3.5 in case of η_{A}. The piecewise minimal interpolation η_{PMred} yields efficiency indices around 2.5 which is significantly better than η_{PMA} and also better than η_{MP1}. The error estimator $\eta_{\mathrm{MP1redCG3}}$ is almost as efficient as the optimal η_{MP1red} with around 2.

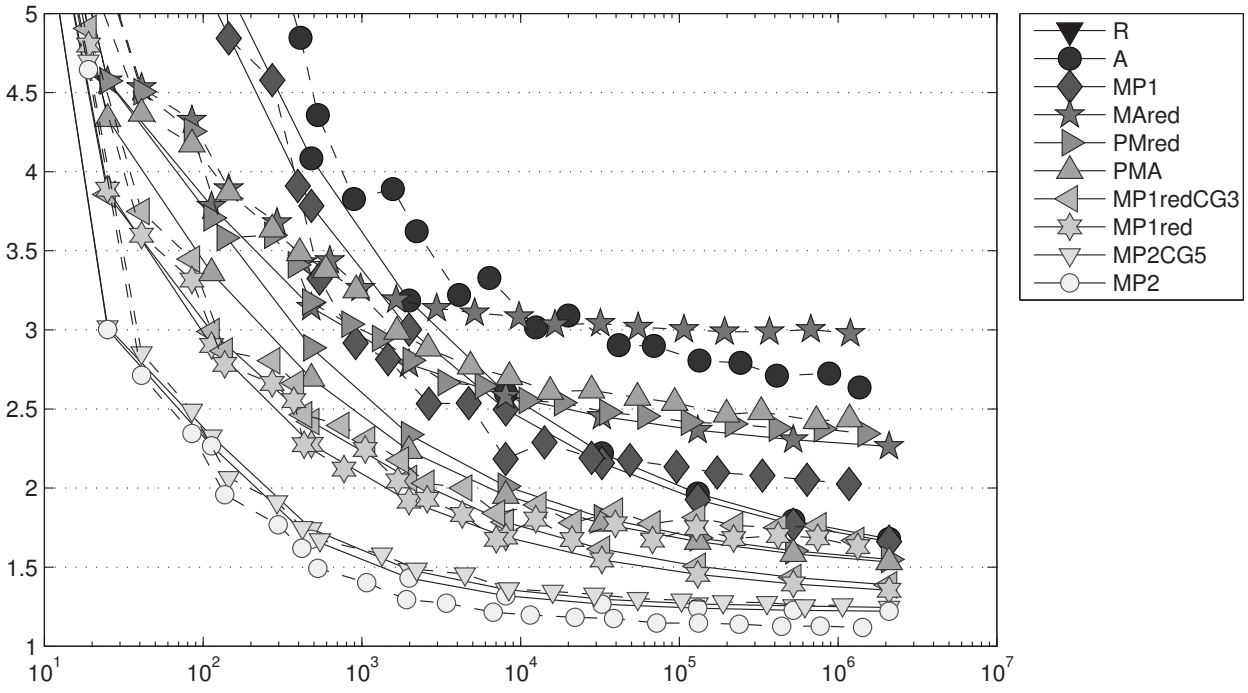

Figure 2. History of efficiency indices $\eta_{\mathrm{xyz}}/|||e|||_{\mathrm{NC}}$ of various a posteriori error estimators η_{xyz} labelled xyz in the figure as functions of the number of unknowns on adaptive (dashed lines) and uniform meshes (solid lines) in Section 5.1.

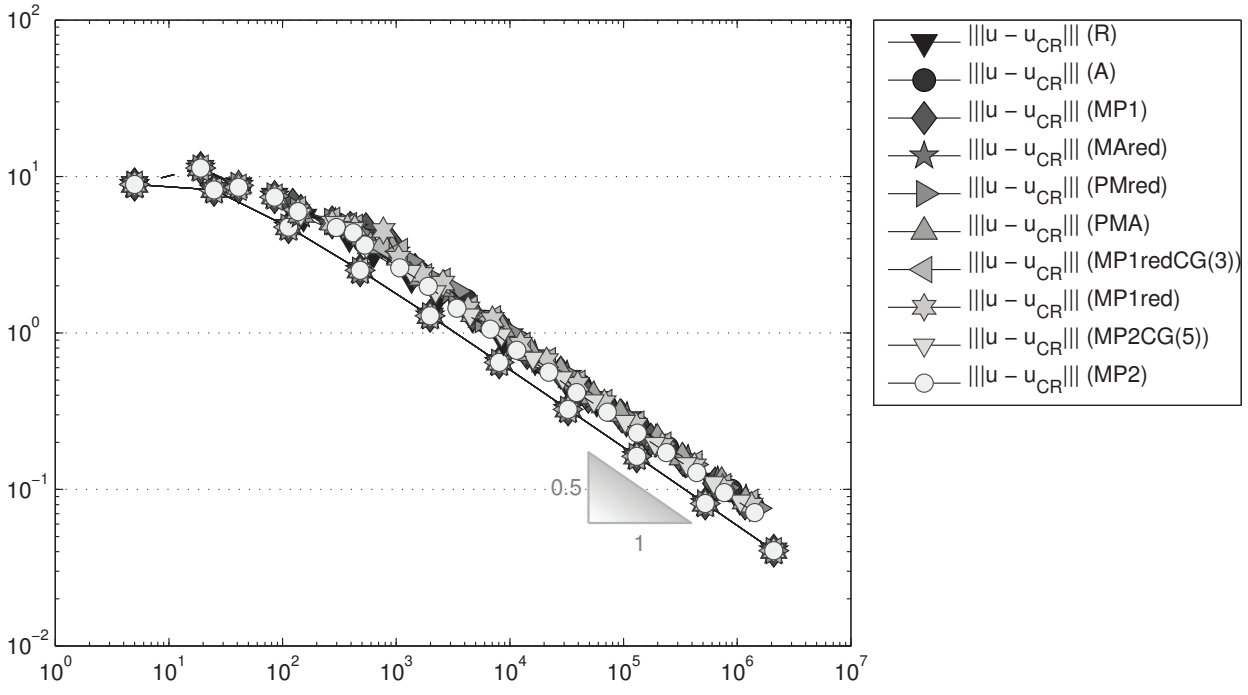

Figure 3. Convergence history of the energy error for uniform (solid lines) and adaptive (dashed lines) mesh refinements in Section 5.1.

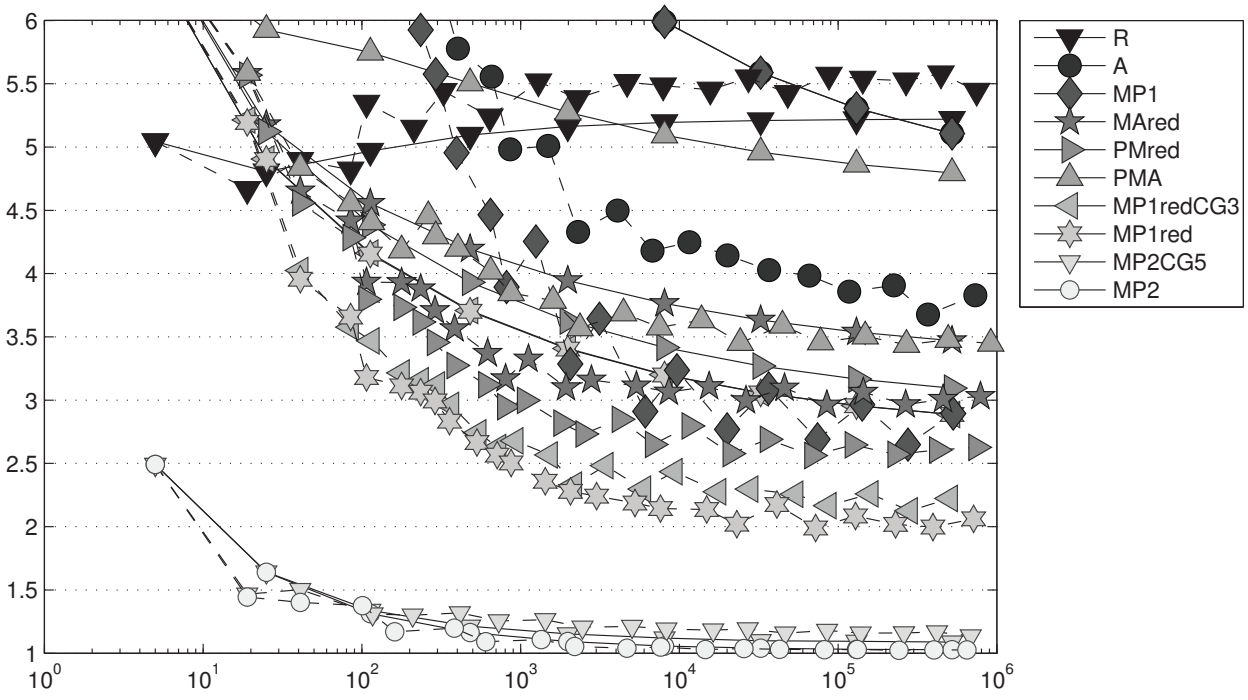

Figure 4. History of efficiency indices $\eta_{\mathrm{xyz}}/|||e|||_{\mathrm{NC}}$ of various a posteriori error estimators η_{xyz} labelled xyz in the figure as functions of the number of unknowns on adaptive (dashed lines) and uniform meshes (solid lines) in Section 5.2.

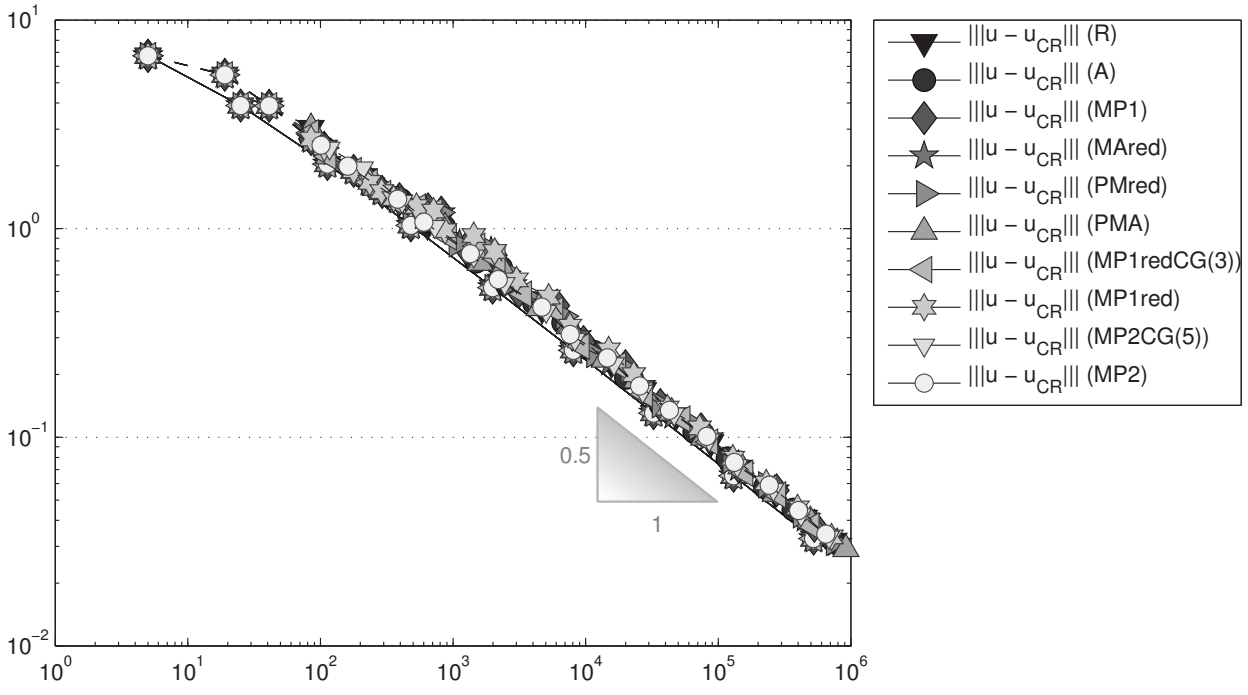

Figure 5. Convergence history of the energy error for uniform (solid lines) and adaptive (dashed lines) mesh refinements in Section 5.2.

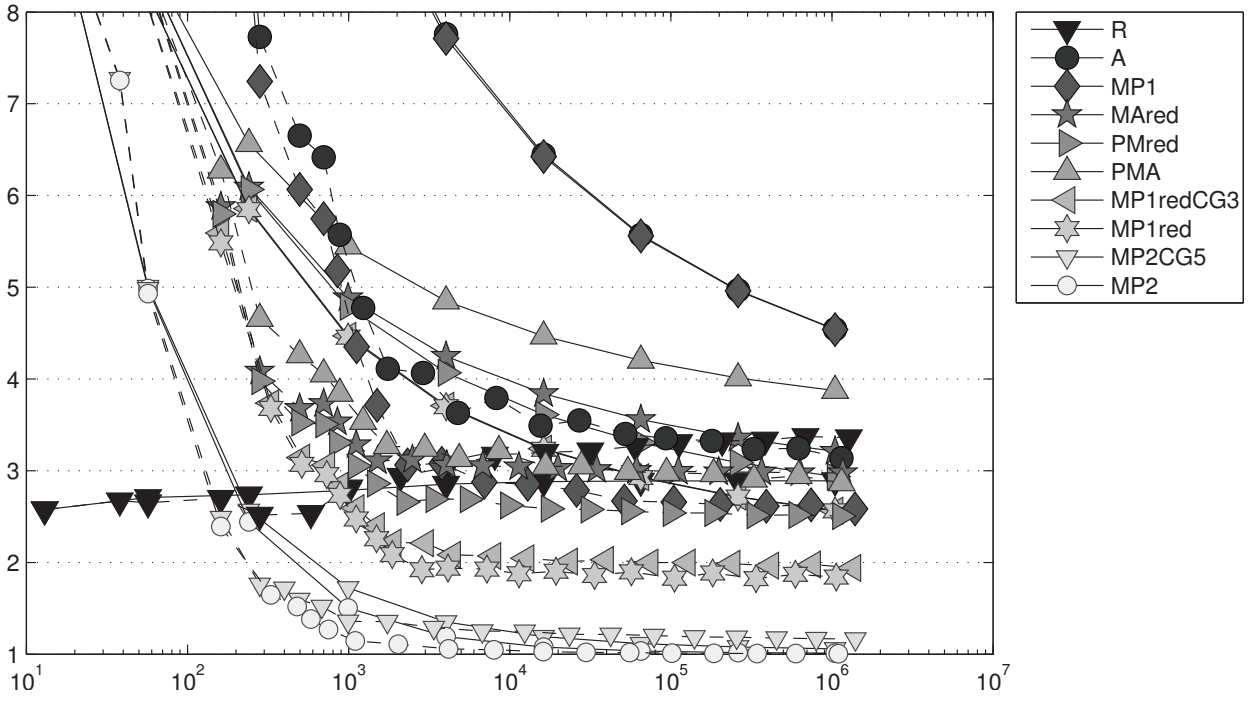

Figure 6. History of efficiency indices $\eta_{\mathrm{xyz}}/|||e|||_{\mathrm{NC}}$ of various a posteriori error estimators η_{xyz} labelled xyz in the figure as functions of the number of unknowns on adaptive (dashed lines) and uniform meshes (solid lines) in Section 5.3.

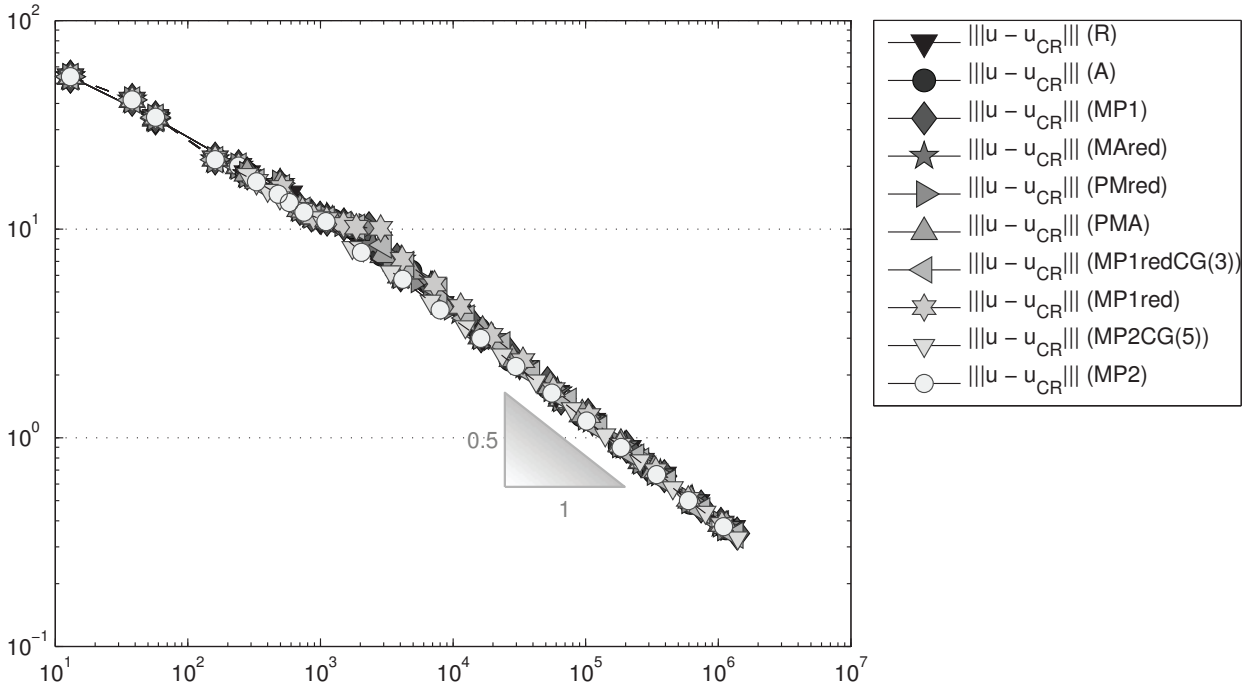

Figure 7. Convergence history of the energy error for uniform (solid lines) and adaptive (dashed lines) mesh refinements in Section 5.3.

5.4. Example on L-shaped Domain

The fourth benchmark problem employs $f(x,y) \equiv 0$ and u_D matching the exact solution

$$u(r,\varphi) = r^\alpha \begin{pmatrix} (\alpha+1)\sin(\varphi)\psi(\varphi) + \cos(\varphi)\psi'(\varphi) \\ -(\alpha+1)\cos(\varphi)\psi(\varphi) + \sin(\varphi)\psi'(\varphi) \end{pmatrix}^T$$

on the L-shaped domain $\Omega = (-1,1)^2 \setminus ((0,1)\times(-1,0))$ with

$$\begin{aligned}\psi(\varphi) = 1/(\alpha+1)\ &\sin((\alpha+1)\varphi)\cos(\alpha\omega) - \cos((\alpha+1)\varphi) \\ &+ 1/(\alpha-1)\ \sin((\alpha-1)\varphi)\cos(\alpha\omega) + \cos((\alpha-1)\varphi)\end{aligned}$$

for $\alpha = 856399/1572864 \approx 0.54$, $\omega = 3\pi/2$ from [21]. For the estimator we set $c_0 = 0.3$ from [19].

Figure 9 shows the convergence history of the energy error for uniform and adaptive mesh refinement. The singularity reduces the convergence speed for uniform mesh refinement significantly. The adaptive mesh refinement algorithm from Section 2.3 leads to the optimal convergence speed, independently of the chosen refinement indicators. This is also true for all other examples so far.

The efficiency indices are displayed in Figure 8 and appear similar to the examples before in the range of 1 to 4.

5.5. Backward Facing Step Example

The last example employs the backstep domain $\Omega = ((-2,8)\times(-1,1)) \setminus ((-2,0)\times(-1,0))$, the right-hand side $f \equiv 0$ and the inhomogeneous boundary data

$$u_D(x,y) = \begin{cases} (-y(y-1)/10, 0) & \text{at } x = -2, \\ (-(y^2-1)/80, 0) & \text{at } x = 8. \end{cases}$$

There is no known reference solution, but the example is well-understood [5, 13]. The error estimators are displayed in Figure 10 for the energy error. Again, optimal minimisation leads to significantly smaller bounds than the local interpolation designs. The employed value $c_0 = 0.3$ might not be a lower bound for the inf-sup constant and so the computed error estimates may not be guaranteed upper bounds.

6. Conclusions

The theoretical and practical results of this paper support the following observations.

6.1. Explicit Error Estimator Sufficient for Effective Mesh Design

The adaptive mesh refinement may be steered by simple η_R-based marking. It does not appear to be favourable to spend more computational time for more laborious refinement rules.

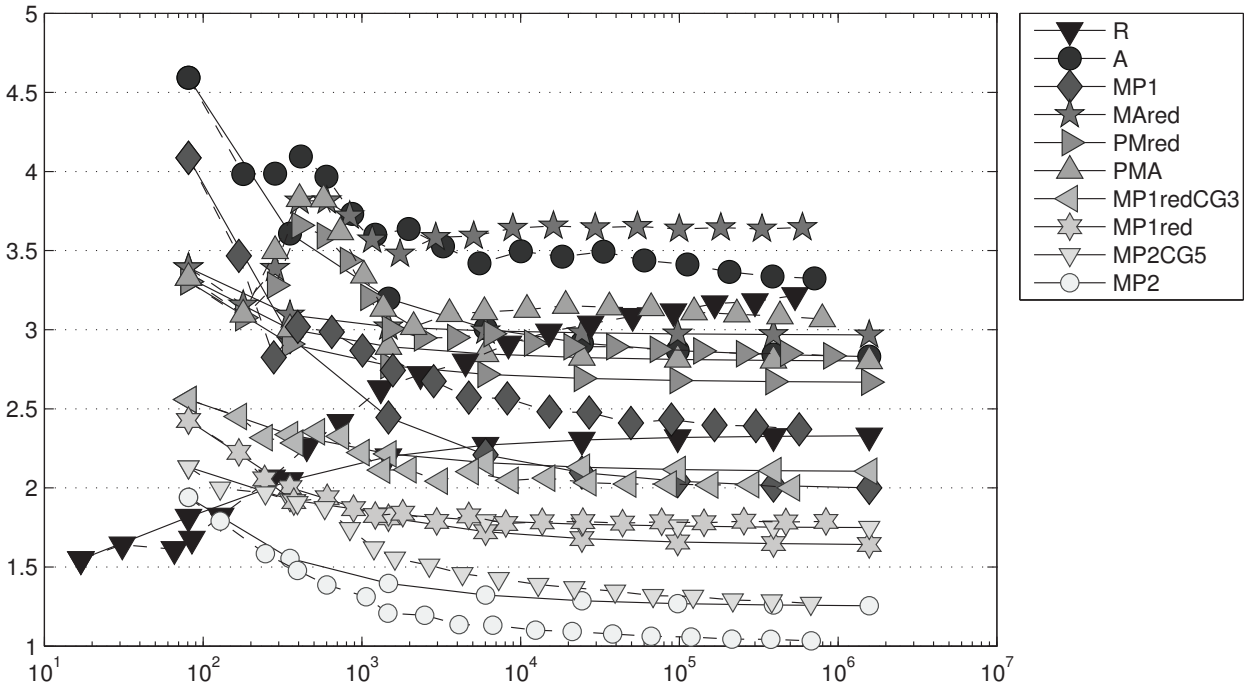

Figure 8. History of efficiency indices $\eta_{\mathrm{xyz}}/|||e|||_{\mathrm{NC}}$ of various a posteriori error estimators η_{xyz} labelled xyz in the figure as functions of the number of unknowns on adaptive (dashed lines) and uniform meshes (solid lines) in Section 5.4.

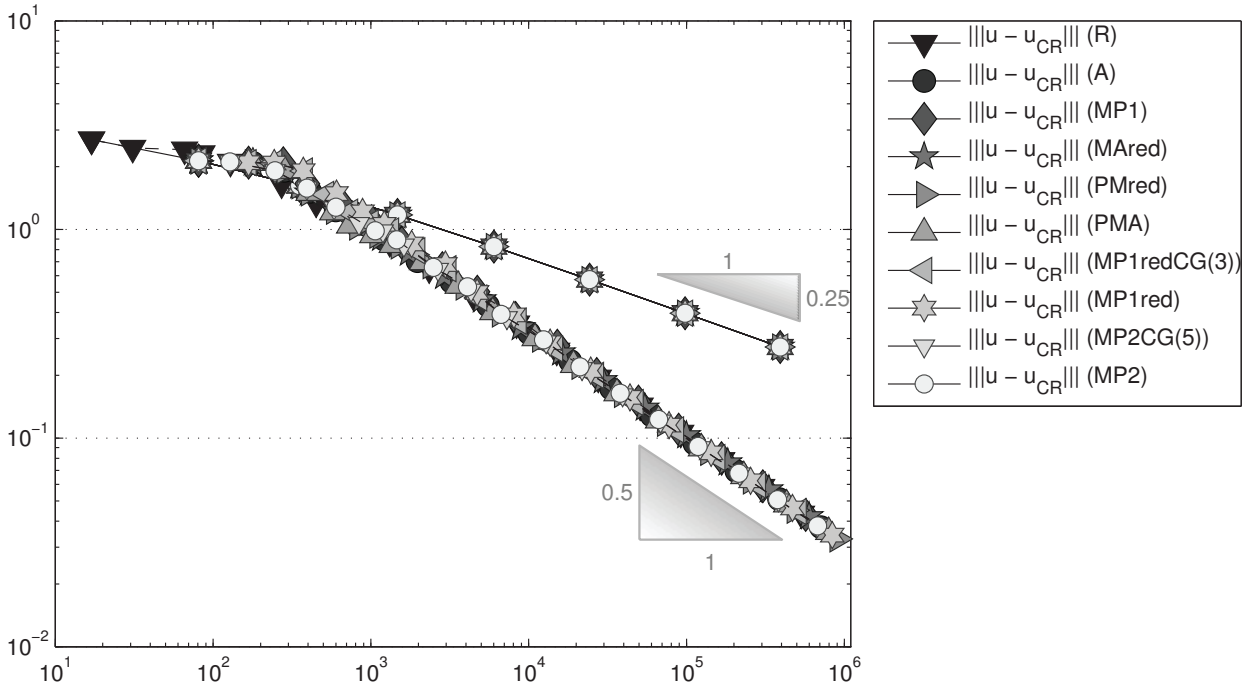

Figure 9. Convergence history of the energy error for uniform (solid lines) and adaptive (dashed lines) mesh refinements in Section 5.4.

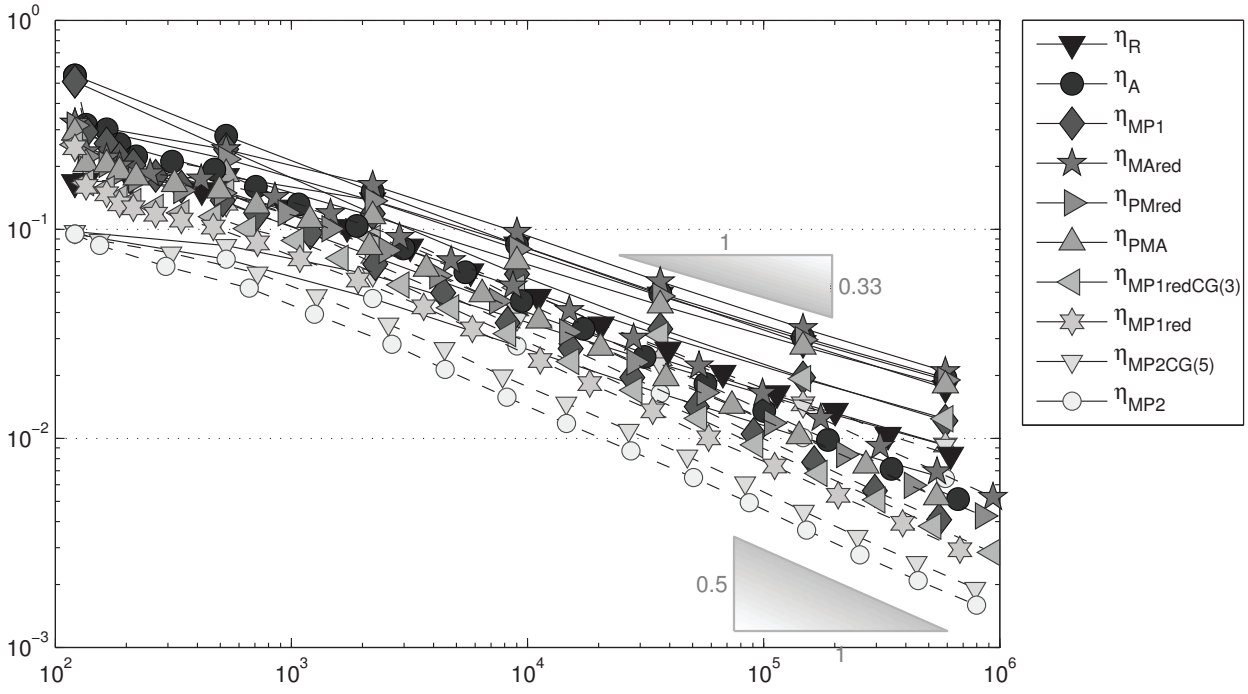

Figure 10. Convergence history of the error estimators for uniform (solid lines) and adaptive (dashed lines) mesh refinements in Section 5.5.

6.2. No Explicit Error Estimation for Reliable Error Control

The explicit residual-based error estimator η_{R} is no guaranteed upper bound for the exact error, since sharp reliability constants are unknown or hard to calculate. The shown efficiency indices for η_{R} are therefore not comparable with those of the other guaranteed error bounds. However, from related situations on the Poisson problem, we expect that the displayed η_{R} from Section 2.3 with $C_{\mathrm{rel}} = 1$ is an optimistic approximation [12,20]. Therefore, the values of η_{R} are plotted in all the figures and display that those explicit residual-based error estimates are less competitive.

6.3. Accurate and Cheap Error Control via η_{PMred}

The experience for Poisson problems in [15] is that the modification v_{red} of v_{A} is superior in all benchmark examples. This is not true for Stokes problems, since η_{A} sometimes is more accurate than η_{MAred}. However, the associated piecewise minimal error estimator η_{PMred} is better than η_{PMA} in all benchmark examples with efficiency indices between 2 and 3.

6.4. Performance of Algorithms 4.1 and 4.2

Since the error estimators of Theorem 3.1, as well as that of [2], involve the sum of norms and not the sum of their squares, some alternating direction minimisation in the variable v and λ is suggested in Algorithms 4.1 and 4.2. The numerical experiments reported in Table 2 suggest that the value $\lambda = 1$ is already a good approximation. Hence, an expensive outer loop over various j does not appear to be necessary in Algorithm 4.1.

6.5. More Accurate Error Control via $\eta_{\mathbf{MP2}}$ or $\eta_{\mathbf{MP1red}}$

Global Minimisation on the red-refined triangulation red($\mathcal{T}$) leads to the error estimator η_{MP1red} with efficiency indices between 1.5 and 2. In most benchmark examples, its approximation $\eta_{\mathrm{MP1redCG3}}$ leads to only slightly less accurate results. However, the optimisation with piecewise quadratic polynomials η_{MP2} allows the best error control with efficiency indices below 1.5, often close to 1. The error estimator η_{MP2CG5} is a very good approximation towards η_{MP2} and even yields better efficiency indices than η_{MP1red}.

6.6. Suggested Approximation of $\eta_{\mathbf{MP1red}}$ with $\eta_{\mathbf{MP1redCG3}}$ or $\eta_{\mathbf{MP2}}$ with $\eta_{\mathbf{MP2CG5}}$

The PCG approximation $\eta_{\mathrm{MP1redCG3}}$ of η_{MP1red} is computed by three iterations of some conjugate gradient scheme with initial value v_{MAred} in direction of the minimiser of the sum of squares. So λ is set to 1 and there is no outer loop of the minimisation as discussed in Section 6.4. The error estimator η_{MP2CG5} also uses the nodal values of v_{MAred} as coefficients for the P_2 ansatz functions on $\mathcal{T}$ and performs five PCG iterations to draw near η_{MP2} with $\lambda = 1$.

Acknowledgments

This work was supported by DFG Research Center MATHEON and by the World Class University (WCU) program through the National Research Foundation of Korea (NRF) funded by the Ministry of Education, Science and Technology R31-2008-000-10049-0. The second author was also supported by the German Academic Exchange Service (DAAD, D/10/44641) during his stay at the Yonsei University in 2010.

References

[1] M. Ainsworth, *Robust a posteriori error estimation for nonconforming finite element approximation*, SIAM J. Numer. Anal., **42** (2004), no. 6, pp. 2320–2341.

[2] M. Ainsworth and W. Dörfler, *Reliable a posteriori error control for nonconformal finite element approximation of Stokes flow*, Math. Comp., **74** (2005), no. 252, pp. 1599–1619.

[3] M. Ainsworth and J. T. Oden, *A Posteriori Error Estimation in Finite Element Analysis*, Wiley, Chichester, 2000.

[4] M. Ainsworth and R. Rankin, *Fully computable bounds for the error in nonconforming finite element approximations of arbitrary order on triangular elements*, SIAM J. Numer. Anal., **46** (2008), no. 6, pp. 3207–3232.

[5] R. E. Bank and B. D. Welfert, *A posteriori error estimates for the Stokes problem*, SIAM J. Numer. Anal., **28** (1991), no. 3, pp. 591–623.

[6] S. Bartels, C. Carstensen, and G. Dolzmann, *Inhomogeneous Dirichlet conditions in a priori and a posteriori finite element error analysis*, Numer. Math., **99** (2004), no. 1, pp. 1–24.

[7] S. Bartels, C. Carstensen, and S. Jansche, *A posteriori error estimates for nonconforming finite element methods*, Numer. Math., **92** (2002), pp. 233–256.

[8] D. Braess, *Finite Elements. Theory, Fast Solvers, and Applications in Solid Mechanics*, Cambridge University Press, New York, 2007.

[9] S. Brenner and L. Scott, *The Mathematical Theory of Finite Element Methods*, 3rd edn., Texts Appl. Math., 15, Springer, New York, 2008.

[10] C. Carstensen, *An adaptive mesh-refining algorithm allowing for an H^1 stable L^2 projection onto Courant finite element spaces*, Constr. Approx., **20** (2004), no. 4, pp. 549–564.

[11] C. Carstensen, *A unifying theory of a posteriori finite element error control*, Numer. Math., **100** (2005), no. 4, pp. 617–637.

[12] C. Carstensen and S. Funken, *Fully reliable localised error control in the fem*, SIAM J. Sci. Comput., **21** (1999), no. 4, pp. 1465–1484.

[13] C. Carstensen and S. A. Funken, *A posteriori error control in low-order finite element discretisations of incompressible stationary flow problems*, Math. Comp., **70** (2001), no. 236, pp. 1353–1381.

[14] C. Carstensen and J. Hu, *A unifying theory of a posteriori error control for nonconforming finite element methods*, J. Numer. Math., **107** (2007), no. 3, pp. 473–502.

[15] C. Carstensen and C. Merdon, *Computational survey on a posteriori error estimators for nonconforming finite element methods for Poisson problems*, J. Comput. Appl. Math., **249** (2013), pp. 74–94.

[16] E. Dari, R. Durán, and C. Padra, *Error estimators for nonconforming finite element approximations of the Stokes problem*, Math. Comp., **64** (1995), no. 211, pp. 1017–1033.

[17] V. John, *A posteriori L2-error estimates for the nonconforming P1/P0-finite element discretization of the Stokes equations*, J. Comput. Appl. Math., **96** (1998), no. 2, pp. 99–116.

[18] R. S. Laugesen and B. A. Siudeja, *Minimizing Neumann fundamental tones of triangles: An optimal Poincaré inequality*, J. Differential Equations, **249** (2010), no. 1, pp. 118–135.

[19] G. Stoyan, *Towards discrete Velte decompositions and narrow bounds for inf-sup constants*, Comput. Math. Appl., **38** (1999), no. 7–8, pp. 243–261.

[20] A. Veeser and R. Verfürth, *Explicit upper bounds for dual norms of residuals*, SIAM J. Numer. Anal., **47** (2009), no. 3, pp. 2387–2405.

[21] R. Verfürth, *A posteriori error estimators for the Stokes equations*, Numer. Math., **55** (1989), no. 3, pp. 309–325.

[22] R. Verfürth, *A Review of A Posteriori Error Estimation and Adaptive Mesh-Refinement Techniques*, Wiley-Teubner Ser. Adv. Num. Math., Wiley, Chichester, 1996.

[23] R. Verfürth, *A Posteriori Error Estimation Techniques for Finite Element Methods*, Numer. Math. Sci. Comput., Oxford University Press, Oxford, 2013.